Study on the mechanism and method of multibeam modulation of planar Lombard lenses

Author:Xiang Guo; Shuxin Wang; Hang Chen

ABSTRACT

Spherical Lombard lenses have wide-angle multibeam performance realization, but their spherical structure makes them inconvenient for practical use and installation. In order to expand the scope of application of the Lombard lens, we planarized the spherical Lombard lens according to the principle of optical transformation, so that it has a regular profile. The excellent gain characteristics of the designed planarized Lombard lens are verified by modeling simulation and comparison with the original spherical Lombard lens. The gain conditions of the planarized Lombard lens are basically the same as those of the spherical Lombard lens, which can greatly reduce the secondary flap, and at the same time, make the electromagnetic wave beam energy converge greatly, so that the communication system is more efficient and energy-saving. However, the planar Lombard lens, which has lost its spherical structure, also loses the undifferentiated focal point characteristic of the Lombard lens, and its beam scanning characteristics are limited. In order to realize a wide-angle multibeam design on planar Lombard lenses, we innovatively designed a super-surface unit capable of changing the beam phase, and verified the controllability of super-surface loading on the beam phase of planar Lombard lenses.

Keywords: Lombard lens; hypersurface; beam deflection; multibeam lens antenna; phase gradient; 3D printing

CONTENTS

Chapter I. Introduction

1.1 Background and significance of the project

With the gradual commercialization of 5G wireless communication system, it can be foreseen that the related millimeter-wave base station layout density will be several times or even dozens of times of the existing base station. Millimeter-wave band electromagnetic wave transmission attenuation is very obvious compared to the microwave band, so it is necessary to improve the antenna gain to achieve coverage depth enhancement. At the same time, millimeter wave antennas also need to have a good angle (width) coverage. In order to realize the required coverage width and coverage depth at the same time, multibeam antennas have become a common solution in 5G and future communication systems. This SRTP project focuses on the design requirements of multibeam antennas, and selects planarized Lombard lens antennas as the research object, based on the surface of the Lombard antenna non-discriminatory focal point characteristics, to achieve the wide-angle multibeam design with the same performance in all directions, and mainly adopts modeling and simulation to study the design method of the planarized Lombard lens antenna and the effect of planarization on the beam, and considers combining with the ultra-surface technology loading scheme to improve the multibeam modulation and transformation capability, and design 1-2 5G antenna prototypes with practicality for verification.

1.2 Technological Route

The main research content of this project includes two parts: studying the design method of planar Lombard lens antenna and the effect of planarization on the beam, realizing large-angle beam scanning and polarization transformation by loading the super-surface, and designing one or two 5G antenna prototypes with practicality for verification. The technical routes for these three parts are as follows:

1、A study of planar Lombard lens antenna design methods and the effect of planarization on beams

Through literature research, we understand the principle and research progress of planarized Lombard lens antenna, learn the surface undifferentiated focus characteristics of Lombard antenna, and use electromagnetic simulation software HFSS to model and simulate to study the design method of planarized Lombard lens antenna and the effect of planarization on the beam. Specifically, based on the invariant deformation of Maxwell's equations under coordinate transformation, the intrinsic parameter matrix of the planarized Lombard lens is designed by using the transformed optics method, and the resulting anisotropic matrix is approximated by the design. The effects of its planarization and the intrinsic parameter matrix approximation on the convergence capacity of the lens and the outgoing wavefront are further analyzed to form a quantitative analytical curve between the planar design parameters and the performance degradation, which is used to guide the subsequent design. In particular, the performance difference between the planar lens normal outgoing wavefront and the original spherical Lombard lens will be systematically compared.

2.Large Angle Beam Scanning and Polarization Transformation by Loading a Super Surface

By designing the hypersurface unit with polarization twisting capability and designing the hypersurface to be loaded on the plane Lombard lens outlet surface, the design of orthogonal

twisting of line polarization, conversion of line polarization and circular polarization is realized. By designing a combined hypersurface with a two-dimensional gradient distribution and designing a hypersurface with an in-plane controllable arbitrary gradient distribution and loading it on the plane Lombard lens exit surface, the beam pointing control is realized to achieve large-angle beam scanning.

3.Designing 5G antenna prototypes with utility validation

Based on the theoretical research content and simulation results in Content 1,,, according to the theoretical lens design parameters derived from calculations and simulations, the equivalent medium method is used to realize the equivalent lens design with 3D printed structures, and all the modeling of the planarized Lombard lens antenna is completed in HFSS by writing script language way. At the same time, the planar feed that matches with the planar Lombard lens is designed as the excitation, and the experimental verification of the planar Lombard lens is completed. On this basis, based on the hypersurface design of content 2, the related physical processing is completed using 3D process, and loaded with the Lombard lens for experimental verification.

1.3 Embodiment of Character and Innovation

1. this project is oriented to the needs of 5G millimeter-wave wireless communication technology, and the research results are expected to have a wide range of applications;

2. the planarized Lombard lens studied in this project has low-profile characteristics and realizes the integrated and integrated design with the feeder;

3. this project adopts the super surface loading technology to enhance the modulation ability of the outgoing beam of the Lombard lens.

Chapter 2 Spherical Lombard Lenses and Planar Lombard Lenses

2.1Principle, design process and result analysis of spherical Lombard lens

2.1.1Design Principle of Spherical Lombard Lens

The Luneburg lens is a spherical lens with a continuous gradual change in refractive index proposed by physicist Luneburg. Light enters the sphere, is continuously deflected according to the change in refractive index, and converges to a point. The same deflection of light by a spherical Luneburg lens can be used to send and receive electromagnetic waves. Due to the spherical symmetry of the ideal Lombard lens, when the position of the feed source is constantly moving on the surface of the Lombard lens, the aperture surface of the outgoing wave is also constantly moving, and it is possible to have a superposition of multiple feed sources on the surface, which leads to an increase in the coverage of the outgoing electromagnetic wave.

The relative permittivity of an ideal Luneburg lens satisfies the relationship $\varepsilon_r = 2 - (\frac{r}{R})^2$,

where RRR represents the maximum radius of the spherical Luneburg lens, and rrr denotes the distance from a point within the lens to the center of the sphere. Since it is impossible to achieve an ideal material with continuously varying permittivity in the real world, the ideal spherical Luneburg lens must be discretized. Theoretically, the more layers a Luneburg lens has, the closer its permittivity approaches continuous variation, resulting in better beam convergence and divergence performance. To verify this theory, we constructed Luneburg lenses with different numbers of layers and used simulations to compare numerical results, confirming that the number of spherical shells significantly impacts gain.

However, even with the discretization of a spherical Luneburg lens, it remains challenging to find materials in the real world that precisely match the required permittivity. Consequently, we decided to miniaturize the Luneburg lens into smaller units. By using the same material and adjusting the duty cycle of each layer, we achieved the desired relative permittivity. In this part of the study, we innovatively proposed using 3D printing technology to fabricate the spherical lens (with the permittivity of the lab's 3D printing material measured at 2.88). A comparison of the gain performance between the small-unit design and the previously uniform-thickness Luneburg lens shows no significant difference. Subsequently, we 3D-printed the small-unit spherical lens, with plans to verify its performance through experiments and compare and optimize it against simulation results.

2.1.2 Design process and result analysis

A discrete layered spherical shell (the innermost layer is a solid sphere) approach is used to approximate the continuous permittivity (refractive index) distribution of an ideal Lombard sphere. Considering that the subsequent work is proposed to be processed by 3D printing, we adopt the equal-thickness spherical shell scheme. According to the ideal Lombard lens formula (r is the average value of the inner and outer radii of each spherical shell layer), the permittivity of each layer can be obtained. The dielectric constants obtained for the innermost and outermost spherical shells roughly satisfy the 1:2 relationship.

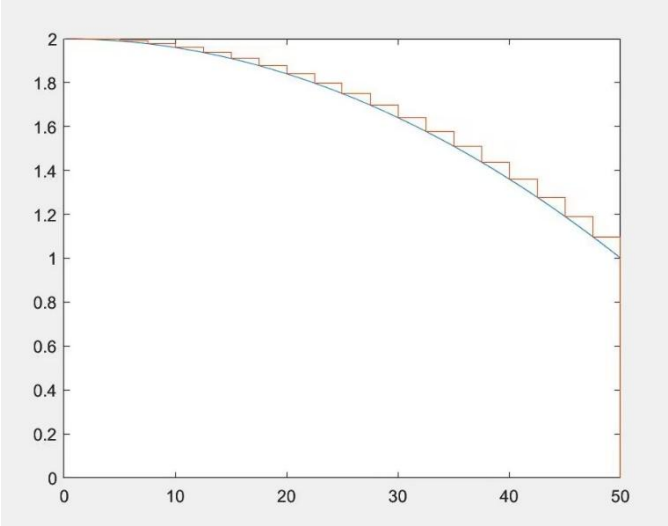

Figure2-1 Fitted curves of dielectric constant and shell thickness averaged over the entire sphere radius of 50 mm

average value of radius(mm)	10.6	10.7	…	47.4	47.5
Corresponding dielectric constant	1.9551	1.9542	…	1.1013	1.0975

Table 2-1 Radius average and corresponding dielectric constant partial data

According to the literature, it is known that the gain profile of the Lombard lens is related to its number of layers; the larger the number of layers, the smaller the discretization error, corresponding to the better convergence of the discrete Lombard spheres realized and the higher the gain. Thus, we chose to model two cases of 7-layer (35 mm radius) and 10-layer (50 mm radius) Lombard lenses with the same thickness of 5 mm for comparative simulations to verify their performance with respect to the number of layers. A larger number than 10 layers is not chosen here because too large a number of layers would lead to a sudden increase in the simulation computational workload and would approach the machining limit leading to machining difficulties. According to the literature, 5-12 layers is a better choice.

The designed Lombard lens operates in the 28 GHz band, so the excitation source is selected to be an open rectangular waveguide of WR28. In order to comparatively illustrate the convergence of the Lombard lens, we first simulate the radiation characteristics of the open waveguide of the excitation source, as shown in the following figure. Its directional earth exhibits an obvious broad beam with a maximum gain of only 6.9 dBi.

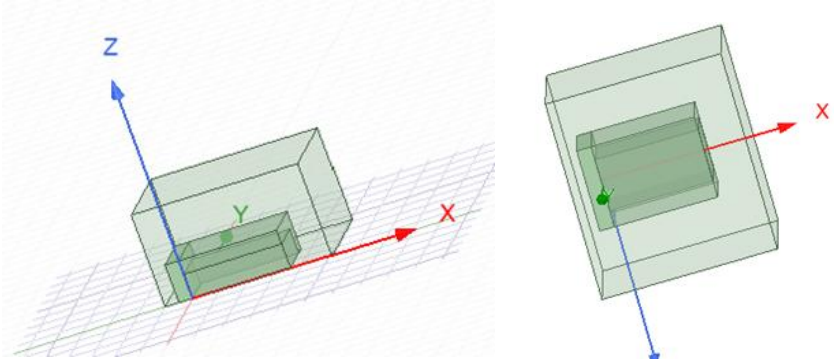

Figure2-2 1/4 rectangular waveguide model vs. complete rectangular waveguide

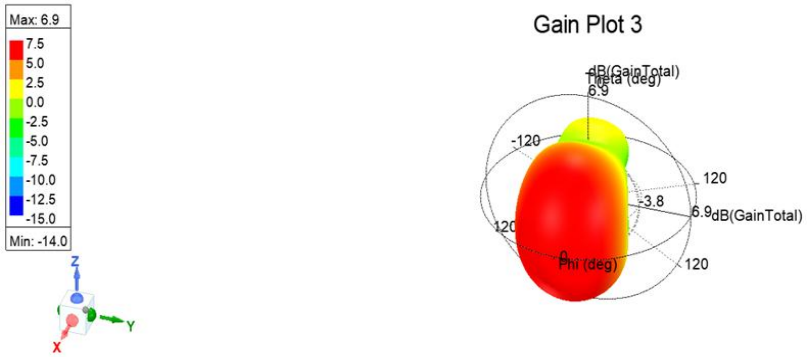

Figure2-3 1/4 Rectangular Waveguide 3D Radiation Map

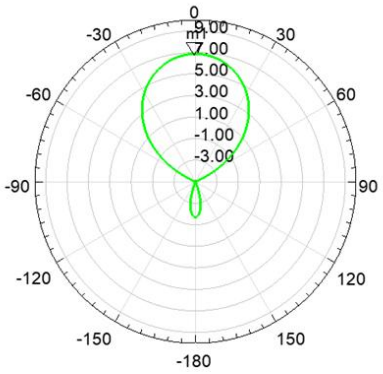

Figure 2-4 1/4 rectangular waveguide H-plane orientation diagram

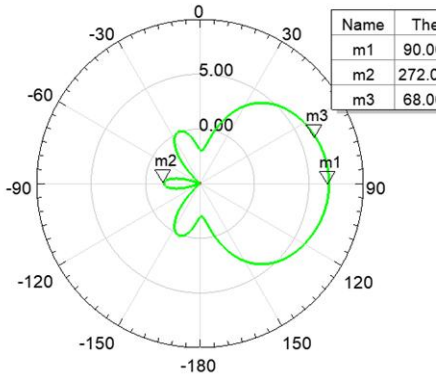

Figure 2-5 1/4 rectangular waveguide E-plane orientation plot

The performance of the excitation feeder with the Lombard lens after the overall simulation is shown below. The gain of the Lombard lens with 7-layer structure is 24.9 dBi, and the gain of the Lombard lens with 10-layer structure is further increased to 27.9 dBi. It can be seen that the Lombard lens enhances the convergence of the radiated waves of the feed source, and the beam width is obviously narrowed. Moreover, the efficiency of the 10-layer Lonber lens is twice as high as that of the 7-layer Lonber lens, and the gain is increased by 3 dB. For this reason, we will adopt the 10-layer design scheme in the subsequent spherical Lonber lens design.

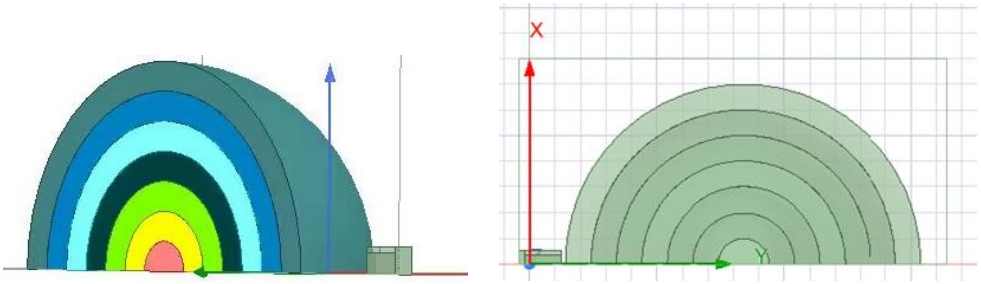

Figure2-6 7 Layer 1/4 Lombard Lens

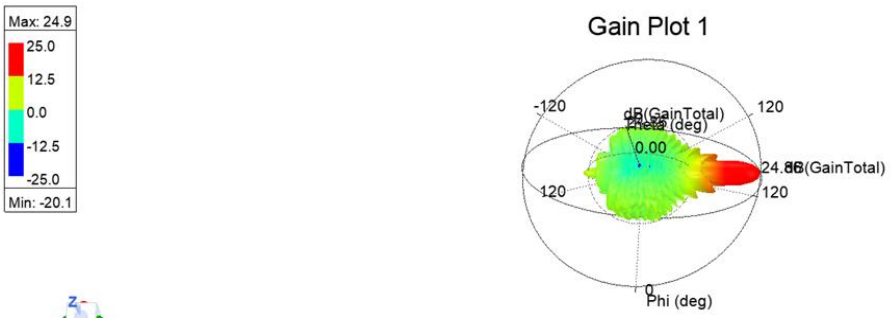

Figure2-7 3D Radiogram of the 7-layer Lombard Sphere

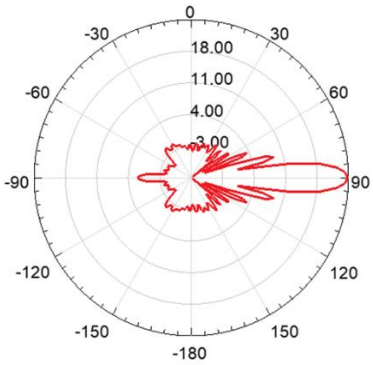

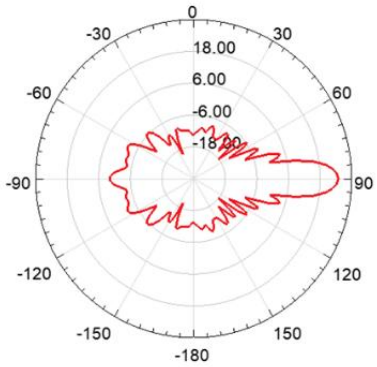

Figure 2-8 H-plane orientation diagram Figure 2-9 E-Side Orientation Chart

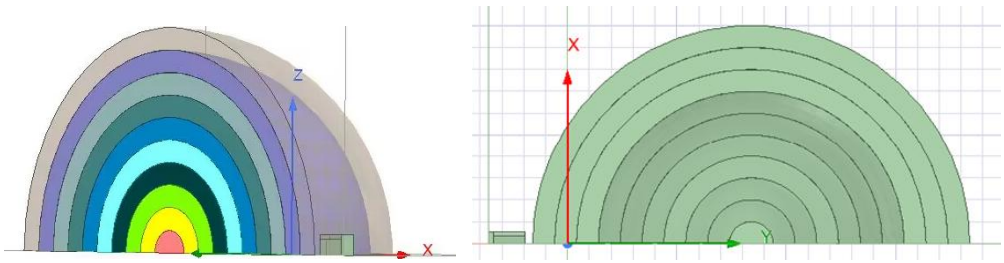

Figure 2-10 10 Layer 1/4 Lombard Lens

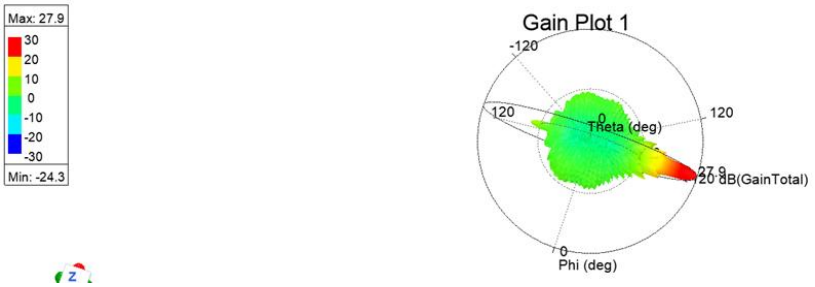

Figure 2-11 3D radiograph of a 10-layer Lombard lens

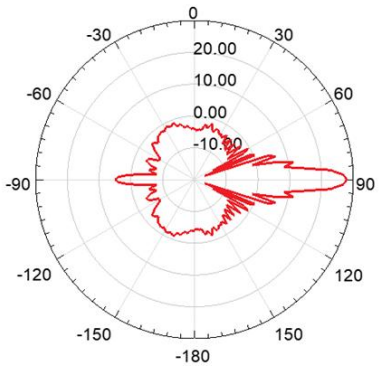

Figure 2-12 H-plane orientation diagram

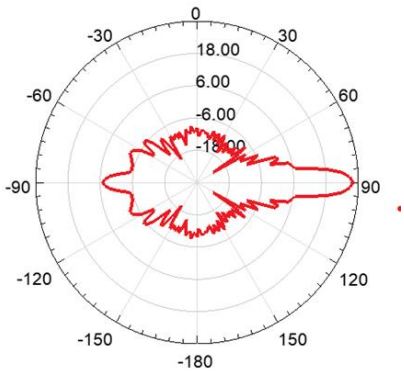

Figure 2-13 E-Side Orientation Chart

And then further consider unitizing the 10-layer ideal discrete Lombard lens. In order to conduct processing experiments on the above designed 10-layer Lombard lens, we propose to innovate the 3D printing process to fabricate Lombard spheres. The chosen 3D printed resin material has a dielectric constant of 2.9 and a loss tangent of 0.0035 (measured in the laboratory). We hope to find a regular, clear structure with a certain degree of stability of the small cell structure, after a large number of data investigation, we choose to replace each layer of the discretized Lombard lens shell with a cubic small cell with a side length of 2mm. Considering that the operating frequency of the Lombard lens is 28 GHz and the wavelength is roughly 10.7 mm, a better approximation can be obtained by selecting the unit with a side length of 2 mm, which does not exceed 1/5 wavelength. The proposed cubic cell is realized by using three mutually orthogonal equal-sized resin material cylinders, and the rest is air. By adjusting the radii of the three cylinders, the modulation of the proportion of air and resin material in the cell can be realized, which leads to the effective tuning of the equivalent dielectric constant. It is chosen to use a three-dimensional orthogonal cylinder structure, whose volume is calculated by Eq:

$$V_{\text{Three orthogonal cylinders}} = (16 - 8\sqrt{2})R^3$$

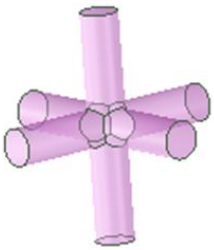

Figure2-14 Proposed unit: three-dimensional orthogonal cylinder

In the formula for calculating the dielectric constant of each layer of an ideal Lombard lens , it is found that the absolute value of the slope gradually increases, and the thickness of the spherical shell takes the value of the middle of the large edge is small. So that the whole ball radius is 50 mm, will r in 0.1 steps respectively calculate the dielectric constant, from which the appropriate value is selected as the corresponding layer dielectric constant, as shown in Table 2-2.

Through the medium air ratio, get the small cell ideal dielectric constant (ε) with the small cylinder radius (R) of the relationship between the formula:

$$\frac{1.9\left(16 - 8\sqrt{2}\right)R^3}{8} + 1 = \varepsilon$$

Due to the error in the volume formula of the orthogonal cylinder, the cylindrical radius needs to be corrected manually on the basis of the original calculation. The correction method is as follows: set the dielectric constant of the 2 mm cube to the corresponding dielectric constant of each layer of the ideal Lombard lens, and then simulate the equivalent orthogonal cylinder with the small cube, compare the s-parameters of the two, and manually modify the range of the difference to be about 2 degrees. The data before and after manual adjustment are:

Number of spherical shells (pcs)	1	2	3	4	5	6	7	8	9	10
Shell thickness (mm)	10	10	6	6	5	4	3	3	2	1
ideal permittivity	1.9900	1.9100	1.7884	1.6636	1.5239	1.3916	1.2775	1.1719	1.0784	1.0199
Cylindrical radius before modification (mm)	0.9617	0.9351	0.8914	0.8417	0.7779	0.7060	0.6294	0.5365	0.4130	0.2615
Cylindrical radius after manual modification (mm)	0.66	0.64	0.57	0.53	0.44	0.38	0.30	0.29	0.18	0.17

Table2-2 Cylindrical radius data before and after modification

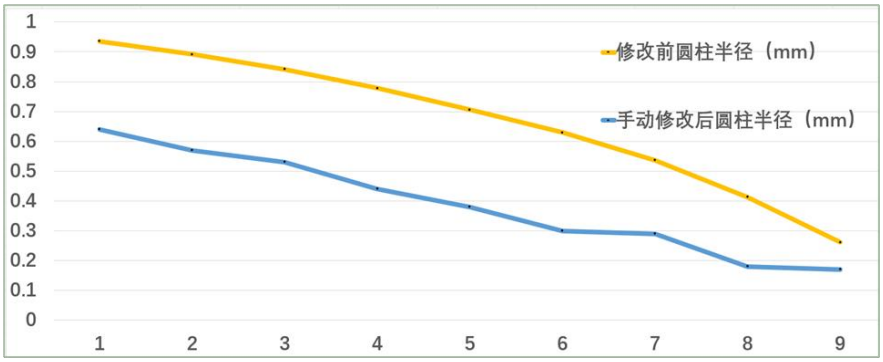

Figure2-15 Comparison before and after manual modification of relative dielectric constant

After modification, the small cells were combined and simulated to obtain a gain of 22.2 dbi, which is about 3 dbi more than the loss gain of the non-equal thickness spherical solid Lobo sphere.

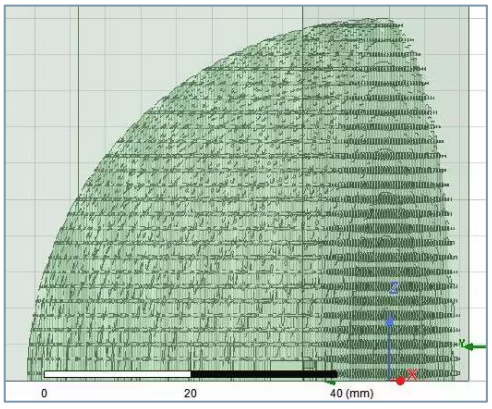

Figure2-16 Lombard lenses after replacing each layer of the spherical shell with cubic small cells

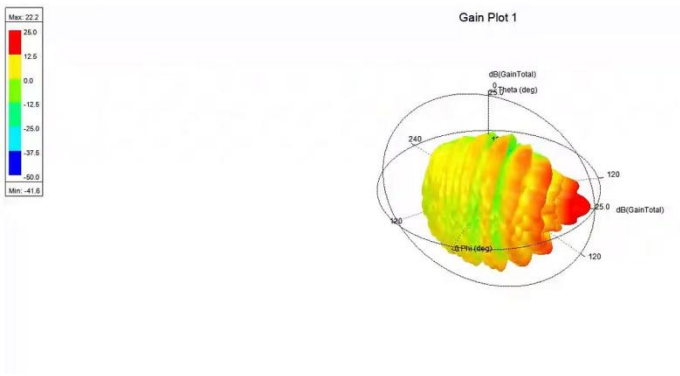

Figure2-17 3D radiographs of small cell equivalent Lombard lenses

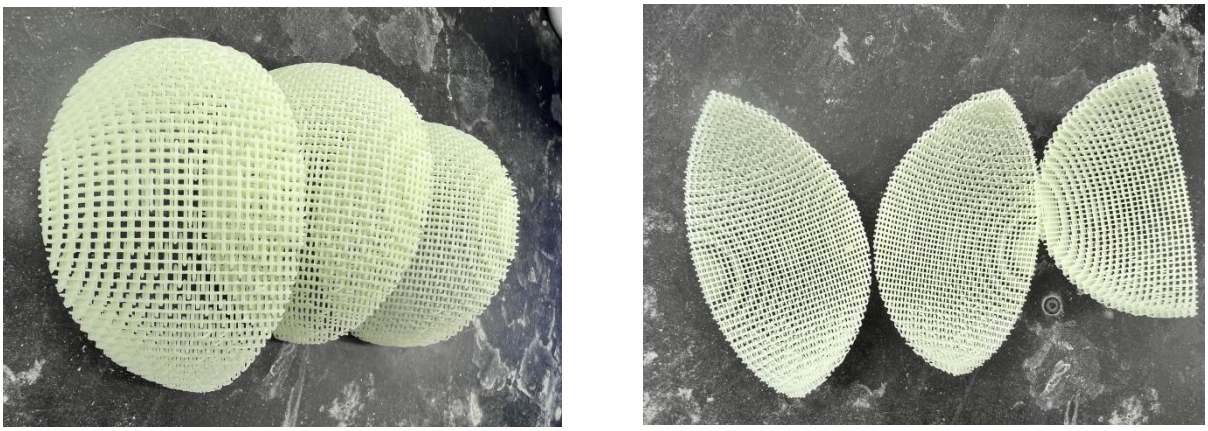

Figure2-18 3D-printed small cell equivalent of a Lombard lens spherical shell (left: outer surface of the spherical shell; right: inner surface of the spherical shell)

2.2 Design process and result analysis of planar Lombard lenses

Spherical Lombard lenses have good geometric symmetry though, making it possible to receive the same size gain at any point on its surface. Meanwhile, due to its special shape, the utilization of spherical Lombard lenses is very limited. Planar Lombard lenses are derived from the geometrical-optical transformations of spherical Lombard lenses, which can be better fixed or placed in any position, but lose the phase tunability of spherical Lombard lenses.

Since the spherical Lombard lens has good geometrical symmetry, it only needs coordinate transformation in two dimensions, and after rotational symmetry the three-dimensional structure can be obtained.

Assume an original coordinate and a new coordinate that has been transformed and then by a Jacobi matrix:

$$\bar{\bar{\Lambda}} = \frac{\partial(x, y, z)}{\partial(x', y', z')}$$

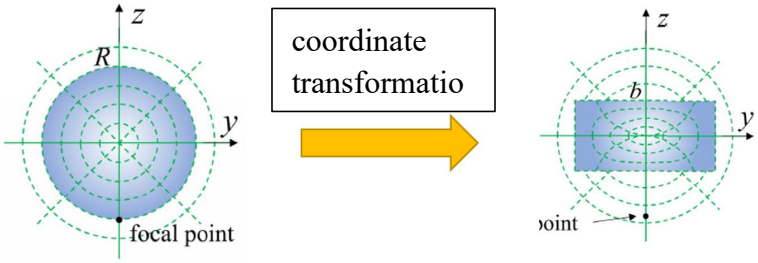

Figure2-19 Spherical Transformation to Planar Graph

The intrinsic parameters of the conversion medium can be calculated as (where and are the relative permittivity and permeability of the medium in the original space, respectively):

$$\overline{\overline{\varepsilon}} = \varepsilon' \frac{\overline{\overline{\Lambda}}\,\overline{\overline{\Lambda}}^{T}}{|\overline{\overline{\Lambda}}|} \quad \overline{\overline{\mu}} = \mu' \frac{\overline{\overline{\Lambda}}\,\overline{\overline{\Lambda}}^{T}}{|\overline{\overline{\Lambda}}|}$$

The Jacobi matrix of the plane transformation is:

$$\overline{\overline{\Lambda}}_2 = \begin{bmatrix} 1 & 0 & 0 \\ 0 & 1 & 0 \\ 0 & \dfrac{zy}{R^2 - y^2} & \dfrac{b}{\sqrt{R^2 - y^2}} \end{bmatrix}$$

Use the above formula to make a graph in MATLAB to show the field quantity distribution of the relative permittivity and magnetic permeability of the planar Lombard lens. (It is usually considered that the magnetic permeability can be neglected after the transformation.) From the figure, it can be seen that after the coordinate transformation of the spherical Lombard lens, the relative permittivity has obvious changes in the xx and yy directions, and the changes in the zz and yz directions are insignificant, and it can be seen that the relative permittivity is large in the middle range, and it gradually decreases in the edge direction from the sectional diagram.

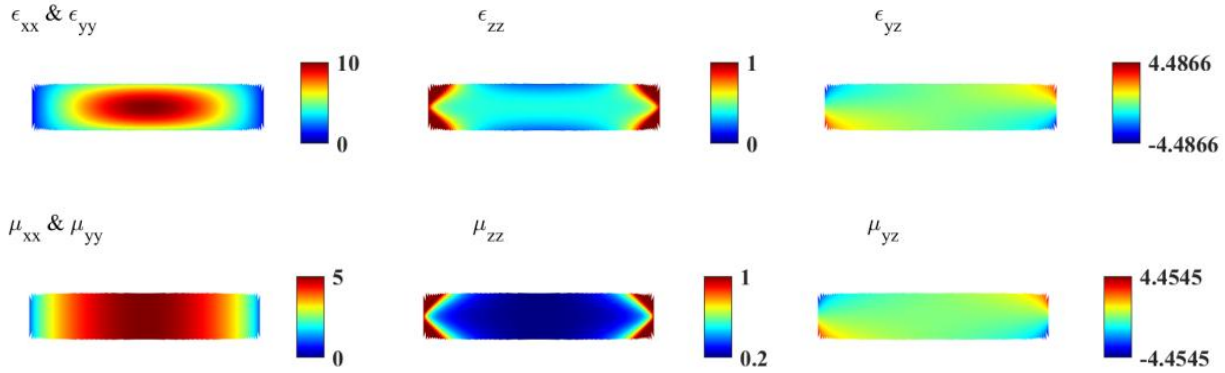

Figure2-20 Plot of planarized dielectric constant intensity obtained through programming

Using the data table obtained after programming, the average values of the radii of each layer of the spherical shell of the original spherical Lombard lens were compared (for the inner diameter and for the outer diameter):

$$r_{\text{flat}} = \frac{r_{\text{inside diameter}} + r_{\text{external diameter (including thickness of the wall)}}}{2}$$

The relative permittivity of each layer of the planarized Lombard lens is obtained as shown in the table below:

Spherical shell planarization serial number	1	2	3	4	5	6	7	8	9	10
Mean value of radius in xO direction	5	15	23	29	34.5	39	42.5	45.5	48	49.5
relative	9.9001	9.1101	7.9398	6.7760	5.5144	4.3542	3.3638	2.4271	1.5098	0.5172

permittivity										

Table2-3 Relative permittivity of the layers of planarized Lombard lenses

Since the planar Lombard lens loses the original spherical symmetry of the spherical Lombard lens, there is only one focal point that can make it achieve the same convergence effect of the spherical Lombard lens. We load plane waves on the air box as shown in Figure 2-21, and find the focal point where the plane waves converge as shown in Figure 2-23, and this focal point is where the feed source of the planar Lombard lens is placed, as shown in Figure 2-24.

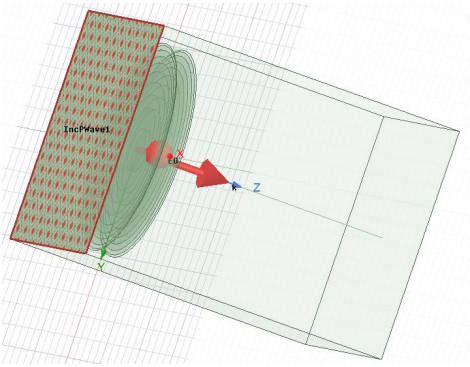

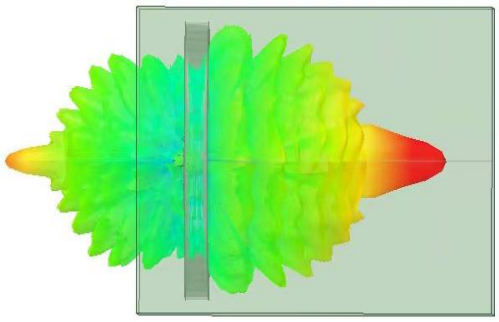

Figure2-21 Finding the Focus of a Spherical Lombard Lens Figure2-223D radiogram of a plane wave projected into a planar Lombard lens

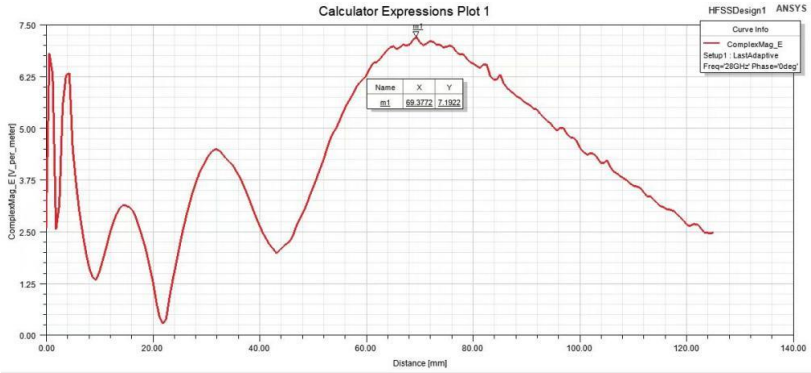

Figure2-23 The focal position is about 69mm from the planar Lombard lens

After finding the focal point, the rectangular waveguide is loaded to the focal point and the gain of the planar Lombard lens is analyzed.

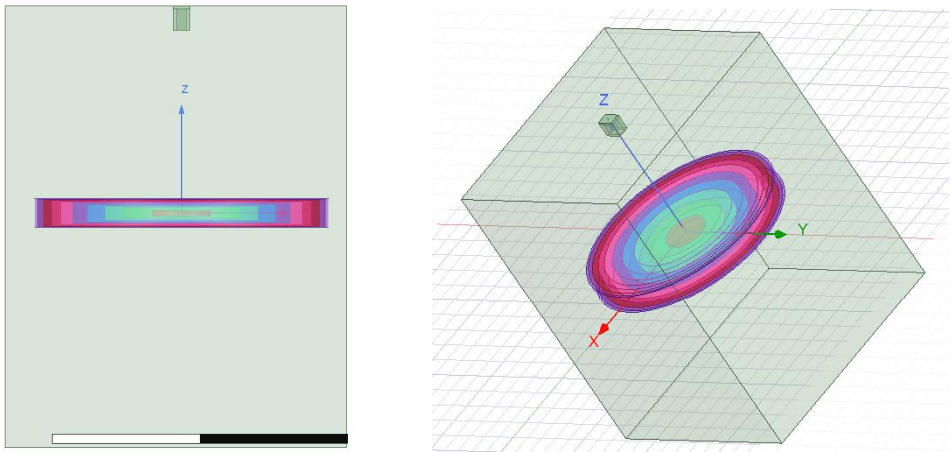

Figure2-24 Planar Lombard lens after loading waveguide

As shown in Figure 2-25, the maximum gain of the planar Lombard lens is 17.8dBi, which is seriously lower than that of the spherical Lombard lens, and the sub-flap situation is serious, analyzing the reason may be that the simulation software is not accurate enough, and the

subsequent use of script software to refine the planar lens to obtain the planar Lombard lens shown in Figure 2-26.

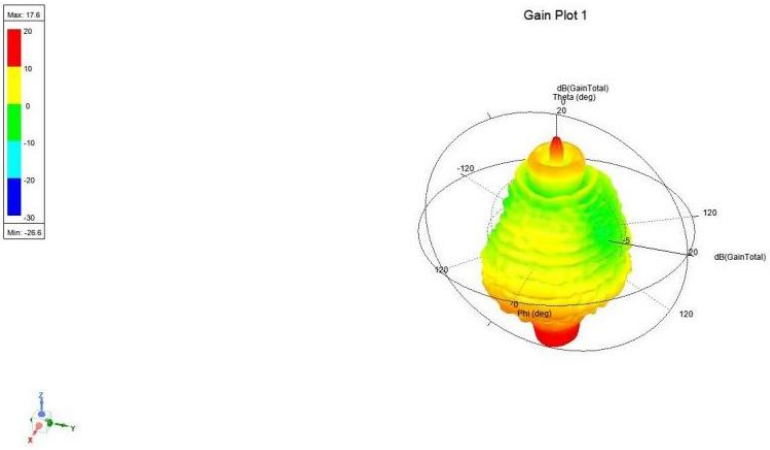

Figure2-25 Planar Lombard Lens Gain Case

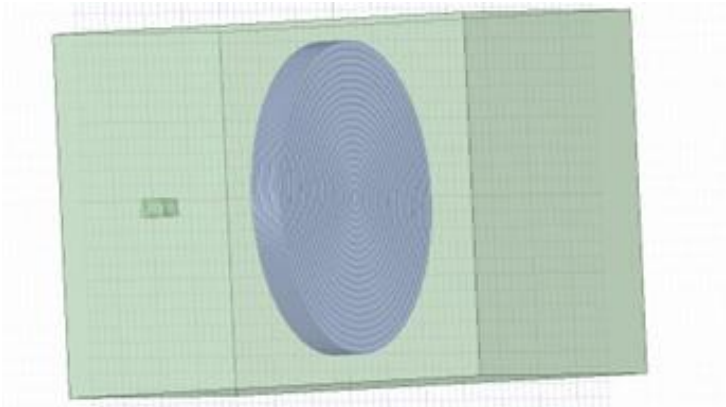

Figure2-26 Planar Lombard lenses after script file refinement

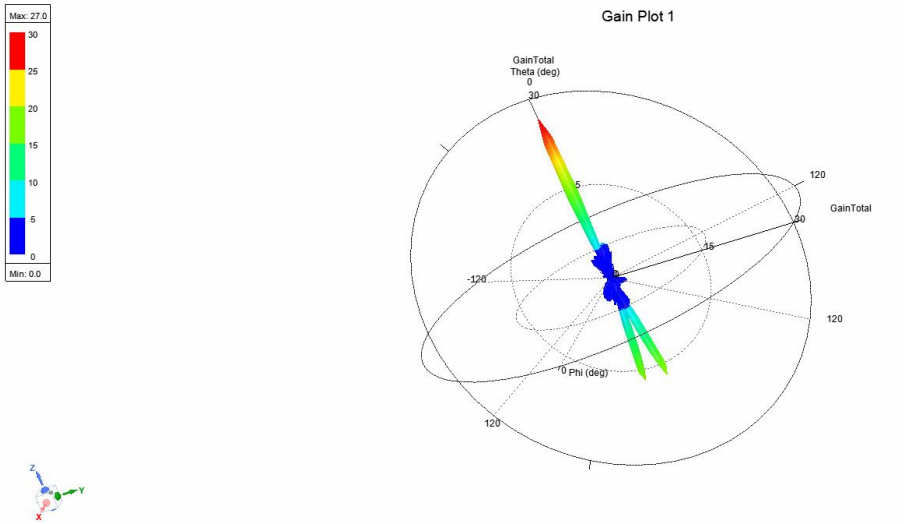

Figure2-27 Gain case of the refined planar Lombard lens

From Fig. 2-27, the final gain of the planar Lombard lens is 27 dBi and there is no significant subflap.

And then we consider unitizing the planar Lombard lens. The dielectric constant of the ceramic sheet material is 9.9, and the small cell structure is a rectangular perforated cell, which replaces the planar Lombard lens with a perforated rectangular cell with a length of 3 mm, a width of 2 mm, and a height of 10 mm, and a perforated rectangle with a length of a, a width of b, and a

height of 10. By adjusting the side lengths of the intermediate rectangular holes, the ratio of the air and ceramic can be adjusted in the cell to achieve the effective equivalent dielectric constant and the gain. realize the effective regulation of the equivalent dielectric constant.

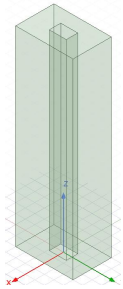

Figure2-28 Proposed unit: Rectangular perforated unit

The equation for the relationship between the ideal dielectric constant (ε) of the small cell and the length (a), width (b) of the perforated rectangle is obtained through the medium-air ratio:

$$9.9 - \frac{8.9ab}{6} = \varepsilon$$

This leads to Table 2-4.

serial number	**1**	**2**	**3**	**4**	**5**
small cell model	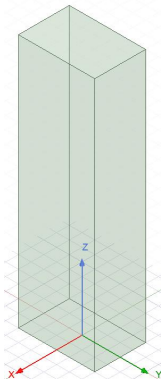	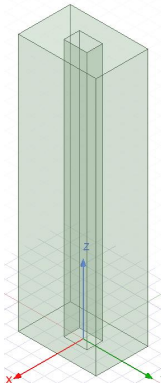	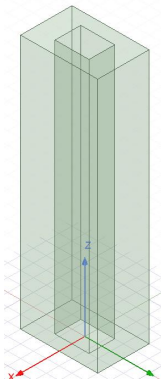	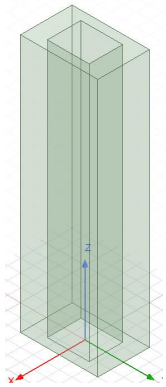	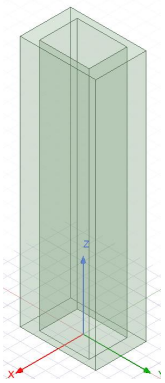
a/mm	0	0.6000	1.0000	1.3000	1.5000
b/mm	0	0.8876	1.3215	1.6200	1.9711
dielectric constant ε	9.9001	9.1101	7.9398	6.7760	5.5144
serial number	**6**	**7**	**8**	**9**	**10**
small cell model	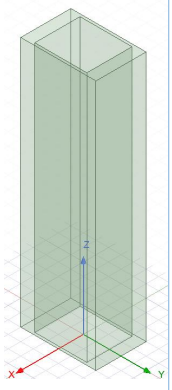	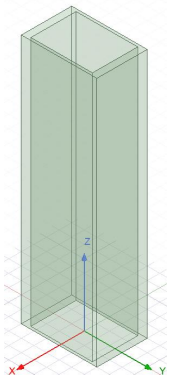	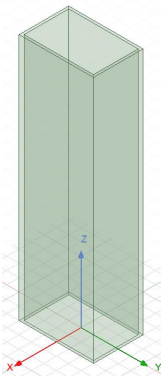	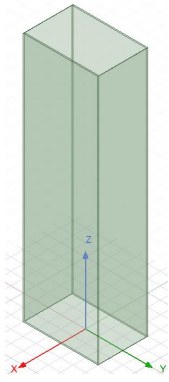	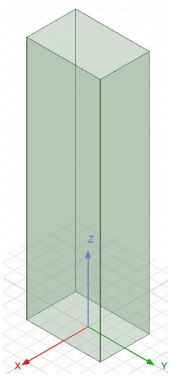
a/mm	1.8000	1.8000	1.8000	1.9000	1.9950
b/mm	2.0771	2.4480	2.7989	2.9770	2.9989
dielectric	4.3542	3.3638	2.4271	1.5098	1.0257

constant ε					

Table2-4 Planar Lombard Lens Equivalent Replacement of Small Cell Size

2.3 Spherical Lombard Lenses vs. Planar Lombard Lenses

From Figure 2-27, the maximum gain of planar Lombard lens is 27dBi, and from Figure 2-11, the gain of spherical Lombard lens is 27.9dBi, which can be seen that the planarized Lombard lens is still able to maintain high gain, and the amplitude of the planar Lombard lens flap is reduced significantly. In conclusion, from spherical to planar, the gain of the Lombard lens is not greatly affected, but it loses the beam phase control function. In order to compensate for this function, we will continue to load the hypersurface on the planar Lombard lens, and utilize the phase gradient of the tangential unit to realize the beam deflection. The planar Lombard lens has the characteristics of small volume and large landing area, which has great utilization value in daily communication, and the study of its gain characteristics is also of significant significance.

Chapter 3 Phase gradient hypersurfaces and beam deflection in planar Lombard lenses

3.1Study of phase gradient hypersurfaces in planar Lombard lenses

3.1.1Phase gradient hypersurface principle

A phase-gradient hypersurface is an anisotropic structure with a subwavelength thickness that enables electromagnetic waves incident on its surface to emit a sudden change in phase and generate a phase gradient in the surface direction. The basic working mechanism of the phase gradient super-surface is that the phase gradient super-surface realizes the phase gradient distribution according to the arrangement of the specially set unit structure, and then the overall phase can be changed so as to control the propagation direction and propagation form of the electromagnetic wave.

If the incident angle of the electromagnetic wave is kept constant and the phase gradient hypersurface at the interface is changed, thus changing the value of the phase mutation, the angle of the transmitted or reflected electromagnetic wave at the interface will be changed to a certain extent, which is a phenomenon known as singular deflection. In the phase gradient hypersurface design process focuses on controlling the phase and amplitude of the unit structure, so it is necessary to ensure that the amplitude of the unit structure is as large as possible in the design process, and the phase coverage of the unit structure is as large as possible to reach 360 ° , so that the corresponding phase distribution reaches the need for certain physical properties.

3.1.2 Modeling process

（1）Phase gradient hypersurface design process

In order to realize a broadband, efficient, and low-loss planar Lombard lens, it is necessary to choose a suitable cell structure and size. In general, the cell structure should have the following characteristics: first, it can provide a sufficiently large phase range (at least 0~360°); second, it can suppress polarization rotation and cross-polarization. Various types of cell structures have been used to design planar Lombard lenses, such as metal patches, metal rings, metal helical coils, dielectric rods, and so on. Among them, the metal patch structure is a commonly used unit structure, which has the advantages of simple structure, large phase range, high reflection efficiency, and small polarization rotation and cross-polarization.

We have designed a metal patch structure, the cross-punched cell, for our study.

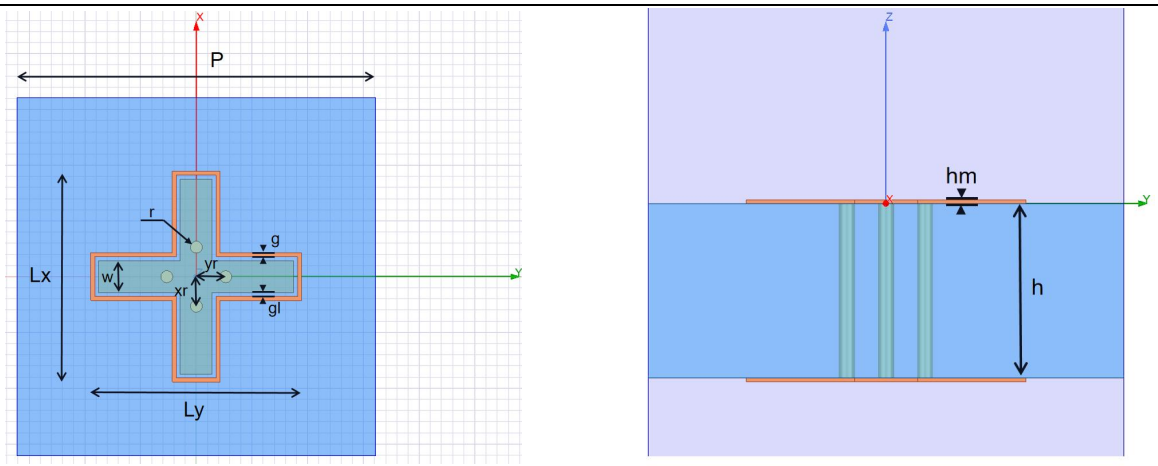

Figure 3-1 Created metal patch structural unit (left: top view, right: side view)

Figure 3-1 gives a schematic diagram of the structure of the hypersurface unit, the whole unit consists of three layers of material, the uppermost layer has a cross-shaped skeletonized metal structure with four holes and a thickness of hm=0.05mm, the length of which is the independent variable Lx, and the width of which is the independent variable Ly, the intermediate dielectric layer is "theRogers RT/duroid 5880 HF plate "(ε_r=2.2) with a thickness of h=2.36mm and the bottom layer is the same cross-shaped skeletonized metal structure with four holes in the upper and lower layers connected by four cylinders. Also, the position of the apertures is related to Lx and Ly, where xr = a*Lx and yr = a*Ly, where "a" is a constant equal to 0.14. The phase shift of the unit cell is obtained by varying the length of the cross dipole from 3.2 mm to 8.2 mm with a resolution of 0.1 mm. Other parametric components of the unit cell are: w = 0.8 mm, gl = 0.1 mm, g = 0.1 mm, and R = 0.15 mm.

In order to achieve polarization diversity, we fixed the structural geometric parameters w, gl, g, r, and adjusted the transmitted phase of the electromagnetic wave by continuously changing the values of Lx, Ly. When we adjust the phase, we first roughly determine the phase corresponding to different Lx sizes through the scanning parameters, and then choose the appropriate phase gradient value according to the phase data table, we choose 80 degrees here, and then refine the size data to find the corresponding nine relative phase-shift values with an error of no more than 5. Here, we choose the nine relative phase-shift values in order to make the phase of the SMD unit cover 0~360 degrees, which is a good way to achieve the This is the necessary condition to realize the broadband, high-efficiency, and low-loss planar Lombard lens.

By continuously optimizing through simulation, we finally adopted nine cross-shaped structures and designed a 10×11 hypersurface with the geometrical parameters of the cell structure shown in Table 3-1. The phase-gradient hypersurface after arranging through a certain arrangement is shown in Fig. 3-2, where each column of cells in the y-direction is of the same kind.

Unit number	1	2	3	4	5	6	7	8	9
Lx	3.6	5.65	6.1	6.6	8.2	5	5.93	6.3	7
S21phase (waves)	-73.4	-151.7	128.4	46.5	-35.9	-113.1	167.6	89.8	9.6
Relative phase shift value	0	-80	-160	-240	-320	-40	-120	-200	-280

Table3-1 Nine geometric parameters of the cross unit structure

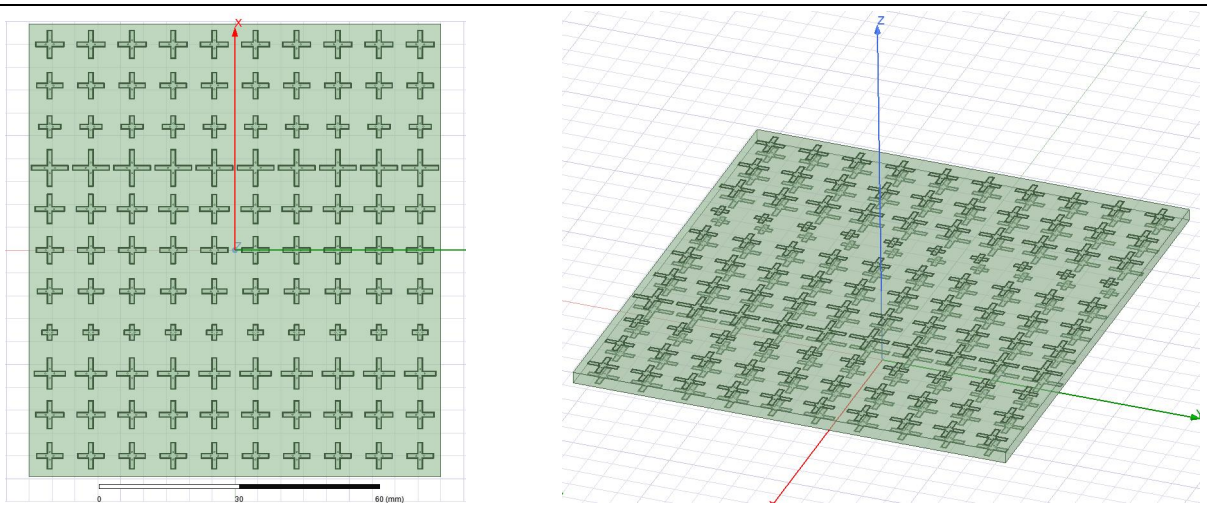

Figure3-2 Schematic representation of the structure after the two-dimensional arrangement of unit structures to form a hypersurface (left: two-dimensional, right: three-dimensional)

（2）Phase gradient hypersurface loading on planar Lombard lenses for simulations

After designing the phase gradient hypersurface, we start to add the hypersurface to the previously designed planar Lombard lens for combination simulation to realize the beam deflection. The specific structure is shown in Figs. 3-3, which are the three-dimensional schematic, side view, and top view of the structural diagram of the phase gradient hypersurface to realize beam deflection, respectively.

In the figure, the phase gradient hypersurface is placed parallel to the plane Lombard lens at a distance of 2 mm from the direction of the plane Lombard lens outgoing wave, the rectangular waveguide is placed at the focal point mentioned in the above paper, and all three are centered on the z-axis.

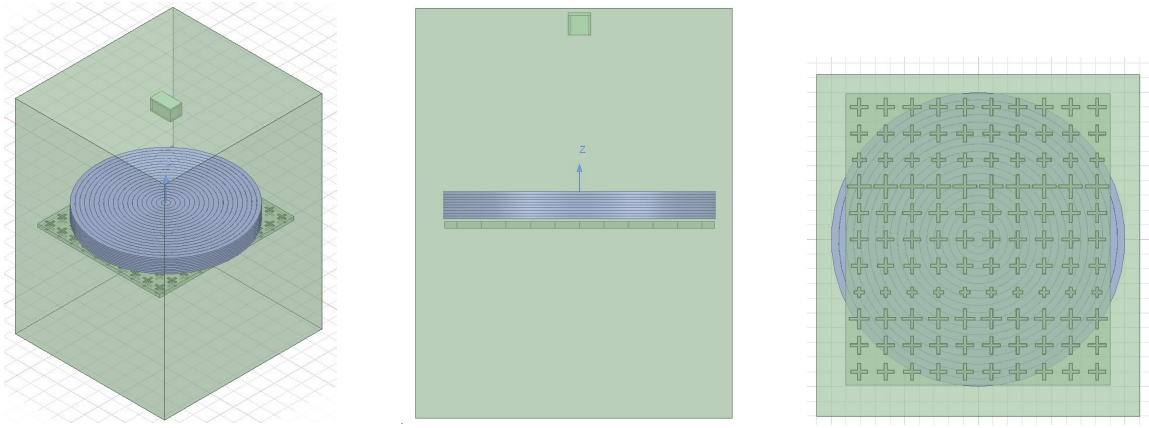

Figure 3-3 Schematic of the simulated structure of the phase-gradient hypersurface to achieve beam deflection (left: 3D, center: side view, right top view)

3.1.3 Simulation results analysis

According to the above model of phase gradient hypersurface loading planar Lombard lens to realize beam deflection, on HFSS software, we simulate the more ideal results, such as Figs. 3-5. From the orientation diagram, we can see that the phase gradient hypersurface makes the beam deflected by 20 degrees and the gain size is 15.7227 dB, which achieves the expected results. From this, we can verify that the phase gradient hypersurface composed of a two-dimensional arrangement of small patch units can make the planar Lombard lens realize beam deflection, thus

realizing the use of the hypersurface loading technology to enhance the modulation ability of the beam emitted from the Lombard lens.

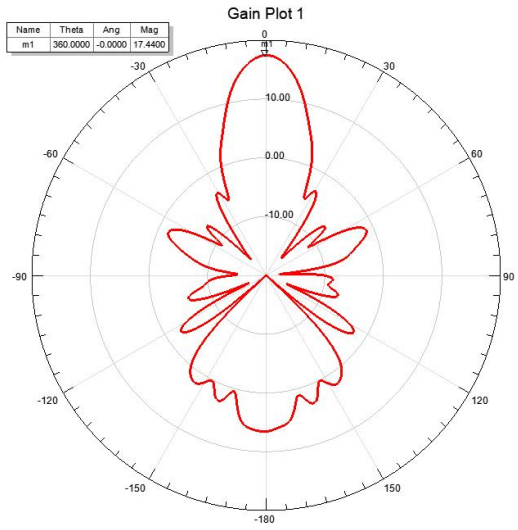

Figure 3-4 Orientation diagram and gain before deflection

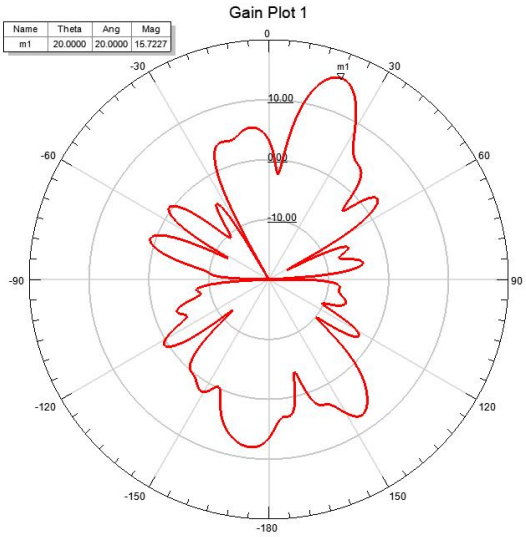

Figure 3-5 Orientation maps and gains for beam deflection achieved by phase gradient hypersurfaces

Conclusion

Spherical and planar Lombard lenses were built and the effect of planarization on gain performance was analyzed. The hypersurface loading to the planar Lombard lens is designed so that the planar Lombard lens realizes the beam deflection control.

Our results are divided into two main parts, the first is to complete the planarization of the spherical Lombard lens, and the second is to load the hypersurface onto the planar Lombard lens and realize the beam deflection.

Our project has certain characteristics and innovations, specifically: when the spherical Lombard lens is planarized, generally the planar Lombard lens no longer has the rotational symmetry property of the spherical Lombard lens, i.e., it is not possible to achieve that the feed antenna, when placed on the surface of the sphere at any point, will have a beam outgoing from the side corresponding to it. Then if we want to do the beam deflection of the planar Lombard lens, the first method is to move the feeder parallel to the surface of the planar Lombard lens, but at this time, the beam deflection will deteriorate, which is manifested in the gain drop, beam broadening, and even some negative flaps may appear, resulting in a large loss. Therefore, we adopt the method of loading phase gradient super-surface to realize beam deflection, at this time, that is, there will not be the loss just mentioned, because at this time only change the phase distribution of the outgoing plane wave, that is, the outgoing phase plane into a slanted plane, because the energy used is unchanged, so theoretically there is no loss of gain, which is the expected result, and has been verified by experiments successfully.

In conclusion, we have achieved beam deflection within a certain angle range while planarizing and reducing the size of the Lombard lens, and at the same time, the gain does not decrease a lot, which is an innovative point and feature that we have achieved.

Reference

[1] X. Che,J. Gao. Research on high-gain planar Lombard lenses[C]// Proceedings of the National Microwave Millimeter Wave Conference 2022 (upper volume), Chinese Institute of Electronics. [Publisher unknown], 2022:4. DOI:10.26914/c.cnkihy.2022.035960.

[2] Yi-Xuan Zheng,Shao-Yong Zheng,Yong-Mei Pan et al. A novel wide-angle scanning planar Lonber lens antenna based on 3D printing[C]// Proceedings of the 2021 Annual National Antenna Conference of the Chinese Institute of Electronics. XI'AN JIAOTONG UNIVERSITY PRESS,2021:4.DOI:10.26914/c.cnkihy.2021.067656.

[3] Yadan Zang,Y.Z. Zhu,X.O. Song et al. Principle of Lombard lens antenna and its research progress[J]. Telecommunications Technology,2021,61(11):1459-1466.

[4] Liu Kun-Ning. Research on the theory and key technology of wide-angle scanning multibeam lens antenna[D]. University of Electronic Science and Technology,2021.DOI:10.27005/d.cnki.gdzku.2021.000222.

[5] Huang M. Research on the theory and application technology of multibeam lens antenna [D]. University of Electronic Science and Technology,2014.

[6] R. Xu and Z. N. Chen, “Note on Transformation-Optics-Based Flat Metamaterial Luneburg Lens Antenna with Zero-Focal Plane,” 2022 International Workshop on Antenna Technology (IWAT), Dublin, Ireland, 2022, pp. 286-288, doi:10.1109/iWAT54881.2022.9810998.

[7] Wang Y. Shell-layer Uber lenses[J]. Radio Engineering,1980(04):68-77.

[8] A.M. Smith ,Lu Biao . Design and application of the Lombard lens[J]. Foreign ship technology. Radar and Countermeasures,1981(07):8-11.DOI:10.19341/j.cnki.issn.1009-0401.1981.07.004.

[9] Warina. Research on multi-mode antenna based on phase gradient hypersurface [D]. Central China Normal University,2023.DOI:10.27159/d.cnki.ghzsu.2022.001838.

[10] Wu, Xianxi. Research on planar array antenna based on phase gradient hypersurface[D]. Guilin University of Electronic Science and Technology,2023.DOI:10.27049/d.cnki.ggldc.2022.001050.

[11] W.T. Che,W.C. Yang,L.Z. Gu et al. Research on multibeam deflection technique of antenna based on hypersurface[J]. Microwave Journal,2022,38(05):7-14.DOI:10.14183/j.cnki.1005-6122.202205002.

[12] Jia Shiyu. Research on beam deflection and polarization conversion based on hypersurface [D]. Xi'an Electronic Science and Technology University, 2022.DOI:10.27389/d.cnki.gxadu.2021.001524.

[13] Guo W.L., Wang G.M., Li H.P. et al. Ultra-broadband phase gradient hypersurface design[J].Microwave

Journal,2016,32(03):51-54+59.DOI:10.14183/j.cnki.1005-6122.201603012.